COMPARATIVE STUDY OF STATE SPACE AVERAGING AND PWM WITH EXTRA ELEMENT THEOREM TECHNIQUES FOR COMPLEX CASCADED DC-DC BUCK CONVERTER

Sangeeta Shete*, Prasad Joshi

Shivaji University, Government College of Engineering, Department of Electrical Engineering, Karad, Maharashtra, India

* corresponding author: sangeetashete2019@gmail.com

Abstract. Until now, most commonly used state space averaging and PWM techniques have been applied to different converter topologies and their advantages and disadvantages were stated. However, the superiority of an analytical technique was not justified based on a parametric comparison of these techniques for the same converter topology. Hence, in this paper, first time a comparative evaluation of two commonly used modelling techniques for fourth order converter is presented. The first approach makes use of a state-space averaging of the converter and is based on analytical manipulations using different state representations of the converter. The second approach is based on PWM switch modelling with an extra element theorem and consists of topological manipulations. The two modelling techniques are applied to the same complex cascaded DC-DC Buck converter and a transfer function is obtained. These techniques are compared for different features and the study concludes that state space modelling technique is systematic and less complicated than PWM switch modelling with an extra element theorem for a higher order converter.

Keywords: Analytical technique, cascaded DC-DC Buck converter, state space averaging, PWM switch modelling, extra element theorem, transfer function.

1. Introduction

Analytical techniques play a vital role in analysing the behaviour of converters under different conditions, performance improvements and design aspects. DC-DC converters have a high number of components and nonlinear behaviour due to the existence of a switch and diode in circuit, which makes them complex in nature. A study of dynamic behaviour and assessment of stability of such nonlinear and complex circuits is a very challenging job. Article [1] presented the review of existing analytical techniques in a structured and meaningful manner and stated that the circuit averaging (CA), state space averaging (SSA), and PWM switch modelling are most commonly used analytical techniques, whereas signal flow graphs, energy factor, switching function, S-Z method are special techniques. SSA is an organised method which allows the inclusion of parasitic elements of a circuit even in the initial stage, permits to explore a linear system with a zero initial condition and nonlinear systems with all initial conditions [2–4]. It is preferred to design a robust controller. However, as it doesn't consider switching frequency in the analysis, this technique is applied by neglecting the ripple effect on inductor current and output voltage [5, 6], which affects its accuracy [7–9]. State space representation is used for mathematical modelling of SEPIC converter, which is further used to contrivance the controller. The results of PI controls and hysteresis controls are compared using PSIM software [10]. The PWM switch modelling technique employs determination of invariant properties of the PWM switch to obtain the average model of circuit and small signal characteristics can be obtained from this average model [11]. PWM technique with conventional approach is simple and pedagogical approach of analysis and provides complete information about steady state and dynamic properties of the converter. This approach is also useful for frequency domain analysis and quasi resonant converters. PWM technique using Extra Element Theorem (EET) is more efficient and practical for general circuits, as it leads to a faster analysis due to a reduced mathematical manipulation, meaningful form of expressions and it is easy to track the errors [12].

An enormous study has been conducted regarding SSA and PWM switch modelling techniques for converters. Article [2] investigated dynamic modelling of Zeta converter, wherein transfer functions, bode plot, transient response and steady state response were obtained using MATLAB and PSPICE. Article [13] obtained state equations and output equations using SSA technique for Buck, Boost and Buck-Boost converter and observed that the state space model simulation results are comparable with a hardware model with a deviation of only 0.0015 V. However, this technique doesn't simulate ripple effect of inductor current and output voltage due to the absence of switching frequency. Article [14] analysed SEPIC converter using an average state-space modelling approach taking into account power losses in converter elements and concluded that this methodology

contributes for converter design as per the requirements and reduces the need for accurate time domain simulations. Mathematical modelling of DC-DC Buck converter using state space averaging and validation of the models was performed using PSIM and MATLAB Simulink [15]. The studies were performed for state space small signal modelling of a double Boost converter integrated with SEPIC converter [3, 16, 17], and SEPIC converter with coupled and uncoupled inductor [18]. Book [19] presented the well-defined and systematic process of small signal analysis of nonlinear circuits using state space analysis to determine the control to output transfer function. The concepts and mathematical modelling of circuits using EET [20] and PWM with EET [21] were studied. The output impedances of three PWM DC-DC converters were analysed in a general and unified manner using PWM switch modelling with EET technique [22]. Article [23] presented the effect of an input filter interaction in the small signal analysis of voltage and current control mode of DC-DC Boost converter and concluded that the methodology is universally adopted. MATLAB Simulink was employed to study the output voltage for multiple DC-DC converters [24] and Boost converter [25].

Article [12] presented PWM with EET to a general circuit and concluded that it is a fast analytical technique which produces a well-ordered polynomial and low entropy form of transfer functions. However, by applying this technique to a complex SEPIC converter, the study concluded that as the circuit becomes complicated, a conventional node and mesh analysis is better instead of the PWM with EET. Nevertheless, the basis of comparison for this statement is not presented in the study, and therefore it is necessary to study the features of PWM with EET technique for higher order circuits. Some of the existing studies have developed the analytical models, obtained simulation results and commented on advantages, disadvantages and applications in a relative manner without comparing the results with a counterpart technique, which doesn't fit into the acceptable scientific and technical approach. The advantages, disadvantages and superiority of a technique should be based on a comparison of two or more techniques for the same converter topology. Even though numerous studies regarding SSA and PWM with EET techniques for different converters have been performed, surprisingly no efforts were done to compare these techniques for the same converter and to comment on the superiority of the analytical technique. The past few years have perceived notable development in the research of DC-DC converter topologies. Although the conversion efficiency of a single-stage converter is better than that of the two-stage converter, the quadratic converters are proposed for extremely large range of conversion ratios. As a part of this, complex cascaded Buck converter (CBC) is always preferred for many applications, as it has a better conversion ratio, high voltage step down ratio, and large voltage regulation [26]. Therefore, in this paper, a comparative evaluation of two widely preferred modelling tools for a higher order DC-DC converter is presented. The first approach makes use of a state-space averaged model of the converter based on the analytical manipulations, whereas the second approach is based on the PWM switch modelling with EET technique based primarily on the manipulations of circuits. The two modelling techniques are applied to a same complex cascaded DC-DC Buck converter and are compared on the basis of their various features to decide the superiority for a higher order circuit.

2. MATERIALS AND METHODS

2.1. COMPLEX CASCADED DC-DC BUCK CONVERTER

The existence of two transistor switches of the conventional cascaded Buck converter can be reduced to a single transistor switch in the complex cascade DC-DC Buck converter as shown in Figure 1, which has two inductors and two capacitors making it a fourth-order circuit and has a quadratic conversion ratio of D^2. This single-transistor realisation is the most additional advantage over a straight forward cascade of two basic converters. The switching section consists of one active switch and three diodes. Though the circuit is complex, the conversion ratio of CBC cannot be realised with less than two capacitors, two inductors, and four switches. However, additional complexity of the converter network may compromise the wide conversion ratio. The control strategy of the complex CBC is depicted in Figures 2a and 2b. The ON state and OFF state correspond to the operation of two Buck converters connected in a cascade as depicted in Figure 3.
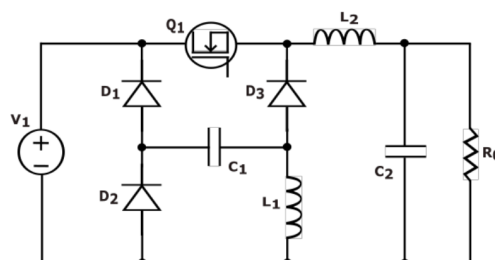

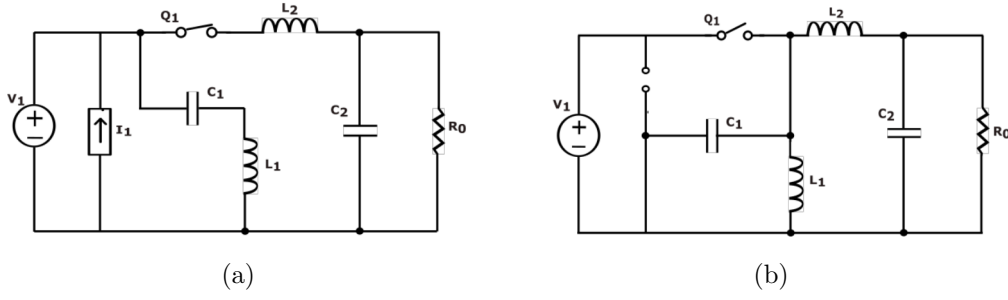FIGURE 1. Topology of cascade DC-DC Buck converter.
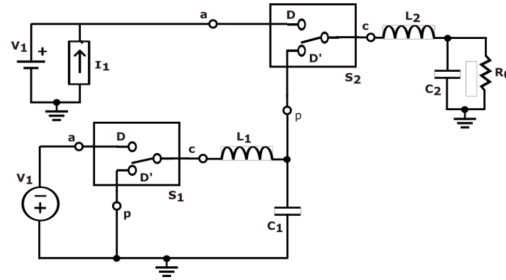
(a)

(b)

FIGURE 2. Switching mechanism of complex CBC.

FIGURE 3. Operation of complex CBC.

The total output voltage is given by Equation 1.

$$V_2 = \frac{1}{T} \int_0^T \left(-DV_1 + DV_1(1+D) \right) \mathrm{dt}$$
$$V_2 = D^2 V_1 \tag{1}$$

Where, D is the duty ratio and

$$D^2 = \frac{1}{T} \int_0^T \check{\mathrm{D}}^2(t)\mathrm{dt}$$

The chopper circuit of CBC has one active switch and three passive switches, which are driven by switching function $\check{\mathrm{D}}^2(t)$ and $\check{\mathrm{D}}'^2(t)$, respectively. The switching function is given as,

$$\check{\mathrm{D}}^2(t) = \begin{cases} 1 & 0 < t < T_{ON} \\ 0 & T_{ON} < t < T \end{cases}$$

2.2. STATE SPACE AVERAGING TECHNIQUE

The state-space averaging method is based on analytical operations for the converter states comprising the determination of linear state model for each possible configuration of circuit and subsequently combining all these elementary models into a single and unified one through a duty factor. The method involves a formulation of the state equation for each state, averaging, perturbation and then rearranging equations to obtain the required transfer function by applying Laplace transform. The complex CBC is considered in continuous conduction mode and switch and diodes are considered in ideal mode. Considering, inductor currents I_{L1}, I_{L2}, and capacitors voltages V_{C1} and V_{C2} as the state variables, the state equation and output equation in ON state of the CBC (Figure 2a) are expressed by the Equations 2 and 3.

$$\left.\begin{array}{l} \dfrac{\mathrm{d}(I_{L1})}{\mathrm{dt}} = \dfrac{V_1}{L_1} - \dfrac{V_{C1}}{L_1} \\ \dfrac{\mathrm{d}(I_{L2})}{\mathrm{dt}} = \dfrac{V_1}{L_2} - \dfrac{V_{C2}}{L_2} \\ \dfrac{\mathrm{d}(V_{C1})}{\mathrm{dt}} = \dfrac{I_{L1}}{C_1} \\ \dfrac{\mathrm{d}(V_{C2})}{\mathrm{dt}} = \dfrac{I_{L2}}{C_2} - \dfrac{V_2}{RC_2} \end{array}\right\} \tag{2}$$

$$V_2 = V_{C2} \tag{3}$$

Similarly, the state equation and output equation in OFF state of the converter (Figure 2b) are expressed by the Equations (4) and (5).

$$\left.\begin{array}{l} \dfrac{\mathrm{d}(I_{L1})}{\mathrm{dt}} = -\dfrac{V_{C1}}{L_1} \\[2mm] \dfrac{\mathrm{d}(I_{L2})}{\mathrm{dt}} = \dfrac{V_{C1}}{L_2} - \dfrac{V_{C2}}{L_2} \\[2mm] \dfrac{\mathrm{d}(V_{C1})}{\mathrm{dt}} = \dfrac{I_{L1}}{C_1} - \dfrac{I_{L2}}{C_1} \\[2mm] \dfrac{\mathrm{d}(V_{C2})}{\mathrm{dt}} = \dfrac{I_{L2}}{C_2} - \dfrac{V_2}{RC_2} \end{array}\right\} \tag{4}$$

$$V_2 = V_{C2} \tag{5}$$

The general form of state equations for ON state and OFF state are given as,

$$\dot{X}(t) = A_1 x(t) + B_1 u(t) \qquad\qquad \text{During dT}$$
$$\dot{X}(t) = A_2 x(t) + B_2 u(t) \qquad\qquad \text{During d'T}$$
$$Y(t) = C_1 x(t) \qquad\qquad \text{During dT}$$
$$Y(t) = C_2 x(t) \qquad\qquad \text{During d'T}$$

Where $X(t)$ is the state vector, $x(t)$ is the state variable matrix, $u(t)$ is the input variable matrix, A_1 and A_2 are the state matrices and B_1 and B_2 are the input matrices, C_1 and C_2 are the output matrices and d is the switching function. Thus, Equations (2) and (3) are represented in matrix form as,

$$\begin{bmatrix} \dot{I}_{L1} \\ \dot{I}_{L2} \\ \dot{V}_{C1} \\ \dot{V}_{C2} \end{bmatrix} = \begin{bmatrix} 0 & 0 & -1/L_1 & 0 \\ 0 & 0 & 0 & -1/L_2 \\ -1/C_1 & 0 & 0 & 0 \\ 0 & 1/C_2 & 0 & -1/RC_2 \end{bmatrix} \begin{bmatrix} I_{L1} \\ I_{L2} \\ V_{C1} \\ V_{C2} \end{bmatrix} + \begin{bmatrix} 1/L_1 \\ 1/L_2 \\ 0 \\ 0 \end{bmatrix} V_1 \tag{6}$$

$$\text{and} \qquad V_2 = \begin{bmatrix} 0 & 0 & 0 & 1 \end{bmatrix} \begin{bmatrix} I_{L1} \\ I_{L2} \\ V_{C1} \\ V_{C2} \end{bmatrix} \tag{7}$$

Equations (4) and (5) are represented in matrix form as,

$$\begin{bmatrix} \dot{I}_{L1} \\ \dot{I}_{L2} \\ \dot{V}_{C1} \\ \dot{V}_{C2} \end{bmatrix} = \begin{bmatrix} 0 & 0 & -1/L_1 & 0 \\ 0 & 0 & 1/L_2 & -1/L_2 \\ 1/C_1 & -1/C_1 & 0 & 0 \\ 0 & 1/C_2 & 0 & -1/RC_2 \end{bmatrix} \begin{bmatrix} I_{L1} \\ I_{L2} \\ V_{C1} \\ V_{C2} \end{bmatrix} + \begin{bmatrix} 0 \\ 0 \\ 0 \\ 0 \end{bmatrix} V_1 \tag{8}$$

$$\text{and} \qquad V_2 = \begin{bmatrix} 0 & 0 & 0 & 1 \end{bmatrix} \begin{bmatrix} I_{L1} \\ I_{L2} \\ V_{C1} \\ V_{C2} \end{bmatrix}. \tag{9}$$

The matrices of Equations (6) to (9) are averaged with respect to switching function D and D' and are given in Equations (10) and (11).

$$A = A_1 D + A_2 D' = \begin{bmatrix} 0 & 0 & -1/L_1 & 0 \\ 0 & 0 & D'/L_2 & -1/L_2 \\ 1/C_1 & -D'/C_1 & 0 & 0 \\ 0 & 1/C_2 & 0 & -1/RC_2 \end{bmatrix} \& B = B_1 D + B_2 D' = \begin{bmatrix} D/L_1 \\ D/L_2 \\ 0 \\ 0 \end{bmatrix} \tag{10}$$

$$C = C_1 D + C_2 D' = \begin{bmatrix} 0 & 0 & 0 & 1 \end{bmatrix} \tag{11}$$

Thus, a complete averaged state space model of the CBC is given by the Equations (12) and (13).

$$
\begin{bmatrix} \dot{I}_{L1} \\ \dot{I}_{L2} \\ \dot{V}_{C1} \\ \dot{V}_{C2} \end{bmatrix} = \begin{bmatrix} 0 & 0 & -1/L_1 & 0 \\ 0 & 0 & D'/L_2 & -1/L_2 \\ 1/C_1 & -D'/C_1 & 0 & 0 \\ 0 & 1/C_2 & 0 & -1/RC_2 \end{bmatrix} \begin{bmatrix} I_{L1} \\ I_{L2} \\ V_{C1} \\ V_{C2} \end{bmatrix} + \begin{bmatrix} D/L_1 \\ D/L_2 \\ 0 \\ 0 \end{bmatrix} V_1 \tag{12}
$$

$$
V_2 = \begin{bmatrix} 0 & 0 & 0 & 1 \end{bmatrix} \begin{bmatrix} I_{L1} \\ I_{L2} \\ V_{C1} \\ V_{C2} \end{bmatrix} \tag{13}
$$

To obtain the linear small-signal state-space model, perturbation is added in each state variables and linear steady state model is obtained as in Equation (14).

$$
\begin{bmatrix} \dot{\hat{I}}_{L1} \\ \dot{\hat{I}}_{L2} \\ \dot{\hat{V}}_{C1} \\ \dot{\hat{V}}_{C2} \end{bmatrix} = \begin{bmatrix} 0 & 0 & -1/L_1 & 0 \\ 0 & 0 & D'/L_2 & -1/L_2 \\ 1/C_1 & -D'/C_1 & 0 & 0 \\ 0 & 1/C_2 & 0 & -1/RC_2 \end{bmatrix} \begin{bmatrix} \hat{I}_{L1} \\ \hat{I}_{L2} \\ \hat{V}_{C1} \\ \hat{V}_{C2} \end{bmatrix} + \begin{bmatrix} -V_1/D'L_1 \\ V_1/D'L_2 \\ -DV_1/2RC_1 \\ 0 \end{bmatrix} \tag{14}
$$

The general equation of Laplace transform of the linear steady state model is given by the following expression,

$$
\hat{x}(s) = [sI - A]^{-1}[(A_1 - A_2)X + (B_1 - B_2)U]\hat{d}(s) = [[sI - A]^{-1}B_d]\hat{d}(s). \tag{15}
$$

For CBC,

$$
(sI - A) = s\begin{bmatrix} 1 & 0 & 0 & 0 \\ 0 & 1 & 0 & 0 \\ 0 & 0 & 1 & 0 \\ 0 & 0 & 0 & 1 \end{bmatrix} - \begin{bmatrix} 0 & 0 & -1/L_1 & 0 \\ 0 & 0 & D'/L_2 & -1/L_2 \\ 1/C_1 & -D'/C_1 & 0 & 0 \\ 0 & 1/C_2 & 0 & -1/RC_2 \end{bmatrix}
$$

$$
(sI - A) = \begin{bmatrix} s & 0 & 1/L_1 & 0 \\ 0 & s & -D'/L_2 & 1/L_2 \\ -1/C_1 & D'/C_1 & s & 0 \\ 0 & -1/C_2 & 0 & s+1/RC_2 \end{bmatrix}. \tag{16}
$$

Now, $\qquad [sI - A]^{-1} = \dfrac{\text{Co-factor of } ((sI - A))^T}{\text{Determinant of } (sI - A)}.$ \hfill (17)

Let, Co-factors of $(sI - A) = \begin{bmatrix} C_{11} & C_{12} & C_{13} & C_{14} \\ C_{21} & C_{22} & C_{23} & C_{24} \\ C_{31} & C_{32} & C_{33} & C_{34} \\ C_{41} & C_{42} & C_{43} & C_{44} \end{bmatrix}$ then,

$$
(\text{Co-factors of } (sI - A))^T = \begin{bmatrix} C_{11} & C_{21} & C_{31} & C_{41} \\ C_{12} & C_{22} & C_{32} & C_{42} \\ C_{13} & C_{23} & C_{33} & C_{43} \\ C_{14} & C_{24} & C_{34} & C_{44} \end{bmatrix}. \tag{18}
$$

Where, co-factors are given in Table 1.

Co-factor	Expression	Co-factor	Expression
C_{11}	$S^3 + S^2\left(\dfrac{1}{RC_2}\right) + S\left(\dfrac{1}{L_2C_2} + \dfrac{D^{'2}}{L_1C_1}\right) + \dfrac{D^{'2}}{RC_1C_2L_2}$	C_{31}	$-S^2\dfrac{1}{L_1} - S\dfrac{1}{RC_2L_1} + \dfrac{1}{C_2L_1L_2}$
C_{12}	$\dfrac{D^{'}}{L_2} - \dfrac{1}{RC_1C_2} - S\dfrac{1}{C_1}$	C_{32}	$-S^2\dfrac{D^{'}}{L_2} - S\dfrac{D^{'}}{RC_2C_2}$
C_{13}	$S^2\dfrac{1}{C_1} - S\dfrac{1}{RC_1C_2} + \dfrac{1}{C_1C_2L_2}$	C_{33}	$S^3 + S^2\left(\dfrac{1}{RC_2}\right) + S\dfrac{1}{L_2C_2}$
C_{14}	$-\dfrac{D^{'}}{C_1C_2L_2}$	C_{34}	$-S\dfrac{D^{'}}{C_2L_2}$
C_{21}	$-S\dfrac{D^{'}}{C_1L_1} - \dfrac{D^{'}}{RC_1C_2L_1}$	C_{41}	$\dfrac{D^{'}}{C_1L_1L_2}$
C_{22}	$S^3 + S^2\left(\dfrac{1}{RC_2}\right) + S\dfrac{1}{L_1C_1} + \dfrac{1}{RC_1C_2L_1}$	C_{42}	$-S^2\dfrac{1}{L_2} - \dfrac{1}{C_1L_1L_2}$
C_{23}	$S^2\dfrac{D^{'}}{C_1} + S\dfrac{D^{'}}{RC_1C_2}$	C_{43}	$-S\dfrac{D^{'}}{C_1L_2}$
C_{24}	$S^2\dfrac{1}{C_2} + \dfrac{1}{C_1C_2L_1}$	C_{44}	$S^3 + S\dfrac{D^{'2}}{L_2C_1} + S\dfrac{1}{C_1L_1}$

TABLE 1. (Co-factors of $(sI - A))^T$.

Determinant of $(sI - A)$ is

$$s\begin{bmatrix} s & -D^{'}/L_2 & 1/L_2 \\ D^{'}/C_1 & s & 0 \\ -1/C_2 & 0 & s+1/RC_2 \end{bmatrix} + 0\begin{bmatrix} 0 & D^{'}/L_2 & 1/L_2 \\ -1/C_1 & s & 0 \\ 0 & 0 & s+1/RC_2 \end{bmatrix}$$

$$+1/L_1\begin{bmatrix} 0 & s & 1/L_2 \\ -1/C_1 & D^{'}/C_1 & 0 \\ 0 & -1/C_2 & s+1/RC_2 \end{bmatrix} + 0\begin{bmatrix} 0 & s & D^{'}/L_2 \\ -1/C_1 & D^{'}/C_1 & s \\ 0 & -1/C_2 & 0 \end{bmatrix}.$$

This yields the determinant of $(sI - A)$ as,

$$1 + s\left(\frac{L_2 + D^{'2}L_1}{R}\right) + s^2[L_2C_2 + L_1C_1 + L_1C_2D^{'2}] + s^3\left(\frac{L_1L_2C_1}{R}\right) + s^4(L_1L_2C_1C_2) \tag{19}$$

Substituting Equations (18) and (19) in (15),

$$[sI - A]^{-1} = \frac{\begin{bmatrix} C_{11} & C_{21} & C_{31} & C_{41} \\ C_{12} & C_{22} & C_{32} & C_{42} \\ C_{13} & C_{23} & C_{33} & C_{43} \\ C_{14} & C_{24} & C_{34} & C_{44} \end{bmatrix}}{1 + s\left(\frac{L_2 + D^{'2}L_1}{R}\right) + s^2[L_2C_2 + L_1C_1 + L_1C_2D^{'2}] + s^3\left(\frac{L_1L_2C_1}{R}\right) + s^4(L_1L_2C_1C_2)} \tag{20}$$

$$\text{and} \qquad B_d = \begin{bmatrix} -V_1/D^{'}L_1 \\ V_1/D^{'}L_2 \\ -DV_1/2RC_1 \\ 0 \end{bmatrix}.$$

Thus, from Equation (14), the equation of Laplace transform of complex CBC becomes,

$$\hat{x}(s) = \tag{21}$$

$$\left\{ \left[\frac{\begin{bmatrix} C_{11} & C_{21} & C_{31} & C_{41} \\ C_{12} & C_{22} & C_{32} & C_{42} \\ C_{13} & C_{23} & C_{33} & C_{43} \\ C_{14} & C_{24} & C_{34} & C_{44} \end{bmatrix}}{1 + s\left(\frac{L_2 + D'^2 L_1}{R}\right) + s^2[L_2 C_2 + L_1 C_1 + L_1 C_2 D'^2] + s^3\left(\frac{L_1 L_2 C_1}{R}\right) + s^4(L_1 L_2 C_1 C_2)} \right] \begin{bmatrix} -V_1/D'L_1 \\ V_1/D'L_2 \\ -DV_1/2RC_1 \\ 0 \end{bmatrix} \right\} \hat{d}(s).$$

The general equation of Laplace transform of the output at a steady state is given by,

$$\hat{y} = C\hat{x}(s) + [(C_1 - C_2)X(s)]\hat{d}(s).$$

From Equation (7) and (9), $C_1 = C_2$. Thus, $\hat{y} = C\hat{x}(s)\hat{d}(s)$.
Hence for complex CBC,

$$\hat{V}_2(S) = \tag{22}$$

$$\begin{bmatrix} 0 & 0 & 0 & 1 \end{bmatrix} \left\{ \left[\frac{\begin{bmatrix} C_{11} & C_{21} & C_{31} & C_{41} \\ C_{12} & C_{22} & C_{32} & C_{42} \\ C_{13} & C_{23} & C_{33} & C_{43} \\ C_{14} & C_{24} & C_{34} & C_{44} \end{bmatrix}}{1 + s\left(\frac{L_2 + D'^2 L_1}{R}\right) + s^2[L_2 C_2 + L_1 C_1 + L_1 C_2 D'^2] + s^3\left(\frac{L_1 L_2 C_1}{R}\right) + s^4(L_1 L_2 C_1 C_2)} \right] \begin{bmatrix} -V_1/D'L_1 \\ V_1/D'L_2 \\ -DV_1/2RC_1 \\ 0 \end{bmatrix} \right\} \hat{d}(s).$$

Solving Equation (23), control to output transfer function of complex CBC is,

$$\frac{\widehat{V}_2(s)}{\hat{d}(s)} = \frac{\left(1 + sL_1\left(\frac{DD'}{2R}\right) + s^2 L_1 C_1\left(\frac{1+D}{2D}\right)\right)}{1 + s\left(\frac{L_2 + D'^2 L_1}{R}\right) + s^2[L_2 C_2 + L_1 C_1 + L_1 C_2 D'^2] + s^3\left(\frac{L_1 L_2 C_1}{R}\right) + s^4(L_1 L_2 C_1 C_2)}. \tag{23}$$

It is realised that the calculation of matrix $(sI - A)^{-1}$ becomes complicated for any high order circuits, which is in agreement with what is stated in [27].

2.3. PWM SWITCH WITH EET TECHNIQUE

The main principle of the PWM switch modelling technique is the elimination of active and passive switches by their time-averaged models and obtain the averaged circuit model for a switched network, which is further inserted into the converter circuit. The final model is a time-averaged equivalent circuit model, where all branch currents and node voltages correspond to averaged values of corresponding original currents and voltages. Replacement of active and passive switches from the basic switch model (Figure 4) by switching functions d and d', respectively, is depicted in Figure 5.
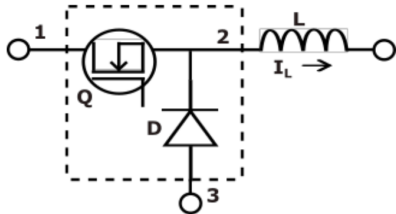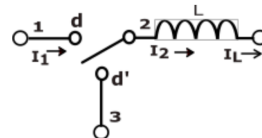

FIGURE 4. Basic circuit model of switch.

FIGURE 5. Replacement of switches.

The invariant average equations for Figure 5 are,

$$\left. \begin{array}{c} I_1 = dI_2 \\ V_{23} = dV_{13} \end{array} \right\} \tag{24}$$

Adding a small deviation in duty ratio function d and then differentiating Equation (24),

$$\left.\begin{array}{l} \hat{\imath}_1 = D\hat{\imath}_2 + I_2\hat{d} \\ \widehat{V}_{23} = D\widehat{V}_{13} + V_{13}\hat{d} \end{array}\right\}, \tag{25}$$

where, D, I_2 and V_{13} are the steady state operating points of PWM switch. The PWM switch model from invariant average Equations (24) is obtained as depicted in Figure 6. Also, using Equation (25), dependent sources $D\hat{\imath}_2$ and $D\widehat{V}_{23}$ are replaced with 1:D transformer and moving control source $\hat{d}V_{13}$ from common terminal side to active terminal side, and the PWM switch model is obtained as in Figure 7. Thus, in PWM switch modelling with EET, the switch and diode are replaced point by point with its equivalent circuit model and further EET is employed to find out TF of the converter circuit.
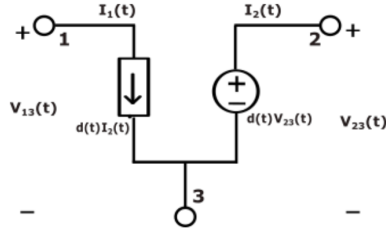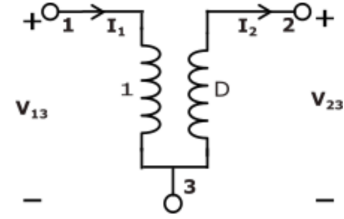

FIGURE 6. PWM switch model.

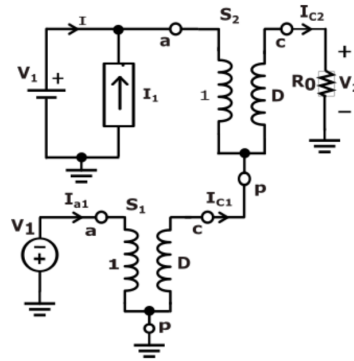FIGURE 7. PWM switch model as 1:D transformer ratio.

FIGURE 8. Two PWM switches as 1:D transformer ratio for CB.

Therefore, for complex CBC, the conditions of ON state and OFF state of switches are employed and two PWM switches are identified, which are represented as S_1 and S_2. The identified PWM switch models are replaced with 1:D transformer along with their small signals as depicted in Figure 8. In order to determine dc operating point of complex CBC, all inductors are short circuited and capacitors are open circuited. Referring to Figure 8, dc operating point with respect to switch S_1 is,

$$V_{ap1} = V_1.$$

Current flowing through terminal 'c' of switch S_1 is,

$$I_{c1} = I_{c2} - DI_{c2} = D^{'}I_{c2}.$$

Similarly, dc operating point with respect to switch S_2 is,

$$V_{ap} = V_1(1 + D),$$

$$I_{c2} = \frac{V_2}{R} = \frac{D^2 V_1}{R}.$$

Once the dc operating point is determined, 4-EET is applied that provides separate, independent steps of the analytical technique. The general form of control to output transfer function is $\left[\frac{\widehat{v}_2(s)}{\hat{d}(s)}\right]$. In the very first step of 4-EET, denominator $\hat{d}(s)$ is determined, for which each impedance element of the converter is treated as extra element and input sources are set to zero. With respect to Figure 3 C_1, C_2, L_2 and L_1 are considered as 4 ports and numbered as port (1), (2), (3) and (4), respectively. Treating these ports as an extra element,

various time constants are determined by removing port elements and observing the remaining circuit through the removed port.

The denominator of the transfer function is given by the following equation:

$$\hat{d}(s) = 1 + a_1 s + a_2 s^2 + a_3 s^3 + a_4 s^4, \tag{26}$$

where

$$
\left.
\begin{aligned}
a_1 &= \tau_1 + \tau_2 + \tau_3 + \tau_4 \\
a_2 &= \tau_1 \tau_1^2 + \tau_1 \tau_1^3 + \tau_1 \tau_1^4 + \tau_2 \tau_2^3 + \tau_2 \tau_2^4 + \tau_3 \tau_3^4 \\
a_3 &= \tau_1 \tau_1^3 \tau_{31}^2 + \tau_4 \tau_4^1 \tau_{41}^2 + \tau_4 \tau_4^1 \tau_{41}^3 + \tau_3 \tau_2^3 \tau_{23}^4 \\
a_4 &= \tau_4 \tau_4^1 \tau_{41}^3 \tau_{413}^2
\end{aligned}
\right\} \tag{27}
$$

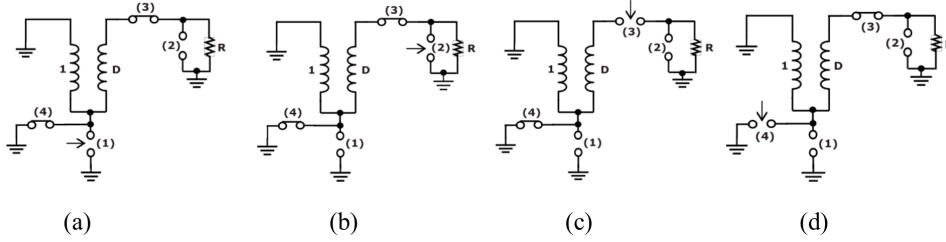Figure 9 is referred for determination of (τ) for a_1, which is explained in Table 2.

$$\text{(a)} \qquad\qquad \text{(b)} \qquad\qquad \text{(c)} \qquad\qquad \text{(d)}$$

FIGURE 9. Determination of (a) τ_1 (b) τ_2 (c) τ_3 (d) τ_4.

τ	Expression
τ_1	Time constant of first port is R_{eq} x C_1, determined by observing the circuit through port (1), capacitor of this port 1 is assumed as extra element and is removed temporarily, L_1, L_2 and C_2 are assumed in dc condition. By observing through port 1, the R_{eq} is 0, therefore, $\tau_1 = R_{eq}$ x $C_1 = 0$.
τ_2	Time constant of second port is R_{eq} x C_2, determined by observing the circuit through port (2), capacitor of this port is now extra element and is removed temporarily, L_1, L_2 and C_1 are assumed in dc condition. After observation, R_{eq} is 0, therefore, $\tau_2 = R_{eq}$ x $C_2 = 0$.
τ_3	Time constant of third port is $\left(\frac{L_2}{R_{eq}}\right)$, which is determined by observing the circuit through port (3). Inductor of this port is extra element and is removed temporarily and C_1, C_2 and L_1 are kept in dc condition. By observation, R_{eq} is R. Hence, $\tau_3 = \frac{L_2}{R}$.
τ_4	Time constant of fourth port is $\left(\frac{L_1}{R_{eq}}\right)$, which is determined by observing the circuit through port (4). Inductor of this port is extra element and is removed temporarily and C_1, C_2 and L_2 are kept in dc condition. By observing the circuit it is seen that R_{eq} is $\frac{R}{D'^2}$. Hence, $\tau_4 = \frac{L_1 D'^2}{R}$.

TABLE 2. Determination of (τ) for a_1.

By summarizing the results of Table 2, we get:

$$a_1 = \frac{L_2}{R} + \frac{L_1 D'^2}{R} \tag{28}$$

First two terms and the last term of the a_2 (Equation (27)) are zero. The calculation of a_2 is only addition of middle terms, i.e. $(\tau_1 \tau_1^4 + \tau_2 \tau_2^3 + \tau_2 \tau_2^4)$, which are indeterminate and is removed by changing the port sequence as $[\tau_4 \tau_4^1 + \tau_3 \tau_3^2 + \tau_4 \tau_4^2]$. Referring the Figure 10, terms τ_4^1 , τ_3^2 and τ_4^2 are determined as described in Table 3.

By summing up the results from the Table 3, we get:

$$a_2 = L_1 C_1 + L_2 C_2 + L_1 C_2 D'^2. \tag{29}$$

The first term of the a_3 (Equation (27)) cannot be determined as it gives a ratio of $(0/0)$, this indeterminacy in time constants is removed with new sequence of ports for a_3 which is,

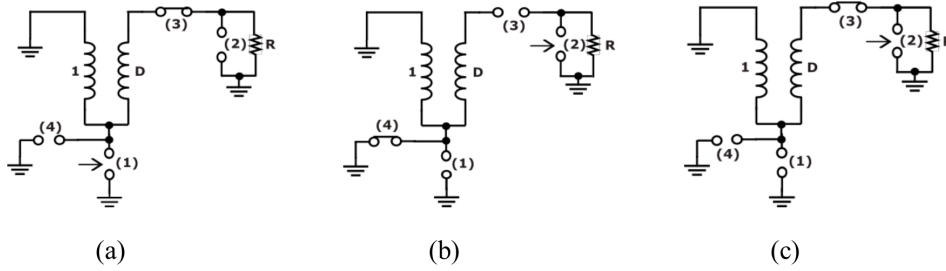$$a_3 = \tau_1 \tau_1^3 \tau_{31}^2 + \tau_4 \tau_4^1 \tau_{41}^2 + \tau_4 \tau_4^1 \tau_{41}^3 + \tau_3 \tau_2^3 \tau_{23}^4. \tag{30}$$

FIGURE 10. Determination of (a) τ_4^1 (b) τ_3^2 (c) τ_4^2.

τ	Expression
τ_4^1	Observing the circuit through port (1), port (4) is considered in high frequency state and ports (2) and (3) are kept in dc condition, capacitor of port (1) is treated as extra element and removed temporarily, equivalent resistance R_{eq} is $\frac{R}{D'^2}$. Hence $\tau_4\tau_4^1 = L_1C_1$.
τ_3^2	Observing the circuit through port (2), port (3) is considered in high frequency state and ports (1) and (4) are kept in dc condition, capacitor of port (2) is treated as extra element and removed temporarily, equivalent resistance R_{eq} is R. Therefore $\tau_3\tau_3^2$ is L_2C_2.
τ_4^2	Observing the circuit through port (2), port (4) is considered in high frequency state and ports (1) and (3) are kept in dc condition, capacitor of port (2) is treated as extra element and removed temporarily, equivalent resistance R_{eq} is R. Therefore $\tau_4\tau_4^2$ is $L_1C_2D'^2$.

TABLE 3. Determination of (τ) for a_2.

The first two terms and last term of the Equation (30) are zero. To calculate τ_{41}^3 , the circuit in Figure 11 is observed through port (3), while ports (1) and (4) are kept in a high frequency condition. Here R_{eq} is R which results in $\tau_{41}^3 = \frac{L_3}{R_{eq}} = \frac{L_3}{R}$. Hence,

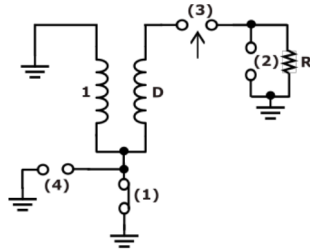$$a_3 = \tau_4\tau_4^1\tau_{41}^3 = \frac{L_1L_2C_1}{R}. \tag{31}$$

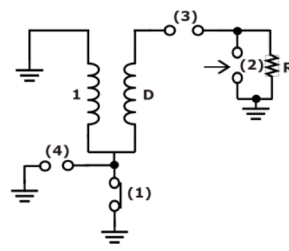
FIGURE 11. Determination of τ_{41}^3.

FIGURE 12. Determination of τ_{413}^2.

For the determination of a_4, referring to Figure 12, τ_{413}^2 is determined by observing the circuit through port (2), while ports (4), (1) and (3) are kept in high frequency condition. In such situation, R_{eq} is R and τ_{413}^2 is RC_2. The calculation of the term $(\tau_4\tau_4^1\tau_{41}^3\tau_{413}^2)$ results in $(L_1L_2C_1C_2)$. Hence,

$$a_4 = L_1L_2C_1C_2. \tag{32}$$

Using Equations (28), (29), (31) and (32) in Equation (26), the denominator of control to output transfer function of complex CBC becomes,

$$\hat{d}(s) = 1 + \left(\frac{L_2}{R} + \frac{L_1D'^2}{R}\right)s + (L_1C_1 + L_2C_2 + L_1C_2D'^2)s^2 + \left(\frac{L_1L_2C_1}{R}\right)s^3 + L_1L_2C_1C_2s^4. \tag{33}$$

Now, the excitation applied to the port is retained as it is and additional excitation is applied to the port of the extra element with the extra element removed. With these two excitations, the response is considered as null. Simultaneously, the conversion ratio D^2 is differentiated with respect to D. Considering this differentiation and null response condition altogether, the numerator of transfer function is determined.
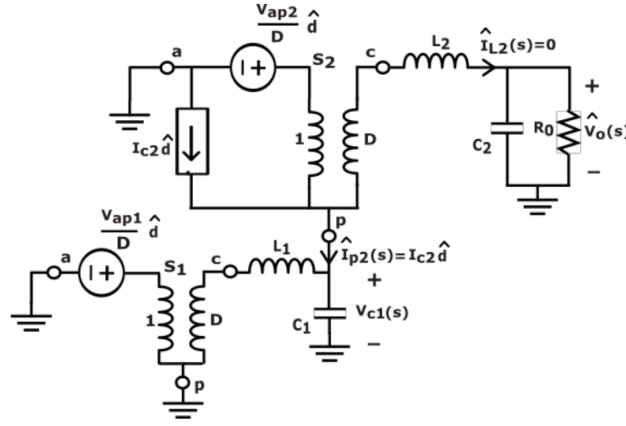
FIGURE 13. Null condition at the output of complex CBC for determination of numerator.

By considering a null response at the output of complex CBC (Figure 13), it is observed that the presence of $\hat{i}_{L2}(s)$ creates the condition as represented by the equation, $\hat{i}_{p2}(s) = \hat{i}_{c2}\hat{d}(s)$ and the resultant voltage across C_1 is,

$$\widehat{V}_{c1}(s) = V_{ap}\hat{d}\frac{(1/(sC_1)}{(SL_1 + 1/sC_1)} + I_{c2}\hat{d}\left[sL_1||(1/sC_1)\right]. \tag{34}$$

This voltage must be the same as that of D side of the second PWM switch. Hence,

$$\widehat{V}_{c1}(s) = -\left[\frac{V_{ap2}}{D}\hat{d} - \widehat{V}_{c1}(s)\right]D. \tag{35}$$

From Equations (34) and (35),

$$D'V_{ap1}\frac{1}{1 + s^2L_1C_1} + D'I_{C2}\frac{sL_1}{1 + s^2L_1C_1} + V_{ap2} = 0. \tag{36}$$

Which yields the numerator of the control to output transfer function of complex CBC as given by,

$$\widehat{V}_2(s) = 1 + sL_1\frac{DD'}{2R} + s^2L_1C_1\frac{1 + D}{2D}. \tag{37}$$

Using Equations (33) and (37), the overall transfer function of complex CBC is given by the Equation (38):

$$\frac{\widehat{V}_2(s)}{\hat{d}(s)} = \frac{\left(1 + sL_1\left(\frac{DD'}{2R}\right) + s^2L_1C_1\left(\frac{1+D}{2D}\right)\right)}{1 + s\left(\frac{L_2 + D'^2L_1}{R}\right) + s^2[L_2C_2 + L_1C_1 + L_1C_2D'^2] + s^3\left(\frac{L_1L_2C_1}{R}\right) + s^4(L_1L_2C_1C_2)}. \tag{38}$$

3. SIMULATION OF COMPLEX CBC

The simulation circuit is developed; voltage and current graphs (Figure 14), time response (Figure 15) and frequency response plot (Figure 16) are obtained for complex CBC using MATLAB simulation to study the behaviour of CBC. The circuit parameters for the simulation are selected as: Inductors $L_1 = 524\,\mu\text{H}$, $L_2 = 1200\,\mu\text{H}$, capacitors $C_1 = C_2 = 5\,\mu\text{F}$, output resistance $R_0 = 8.05\,\text{ohm}$, switch (Q_1) parameters: FET ON resistance = $0.1\,\Omega$, internal diode resistance = $0.01\,\Omega$, internal diode forward voltage = $0.7\,\text{V}$, diode (D_1, D_2, D_3) parameters: resistance = $0.01\,\Omega$, forward voltage = $0.8\,\text{V}$, switching frequency = $50\,\text{KHz}$.

For a duty ratio of 0.35, input voltage $V_1 = 25\,\text{V}$, and source current = $0.05746\,\text{A}$, output voltage $V_2 = 3\,\text{V}$ and load current = $0.367\,\text{A}$ was observed (Figure 14). Also output voltage and load currents for different duty ratios of complex CBC are depicted in Table 4. From the transient and steady state response, it is observed that the output voltage has settled to about 3 volts with the settling time of approximately $0.9\,\text{ms}$ after the application of input voltage. The system is stable (Figure 16), as gain margin is positive ($\infty\,\text{db}$) and phase margin is also positive (450°).
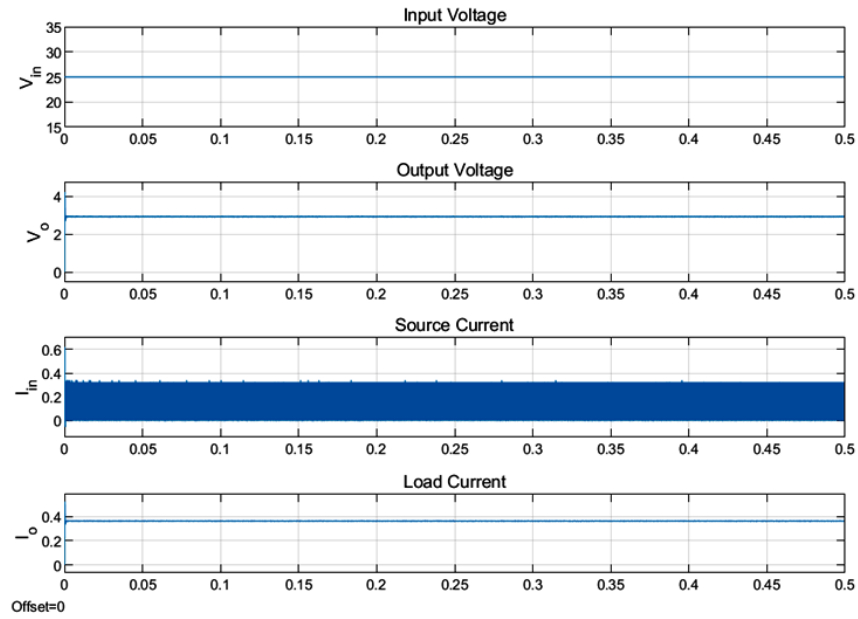
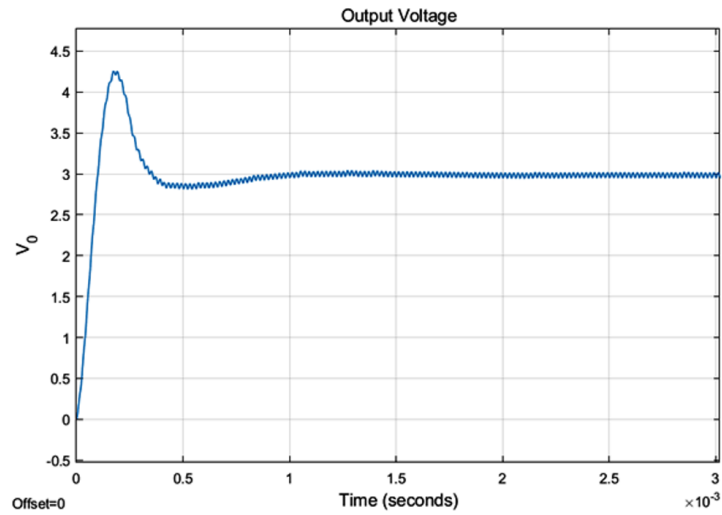FIGURE 14. Voltage and current graphs of complex CBC.

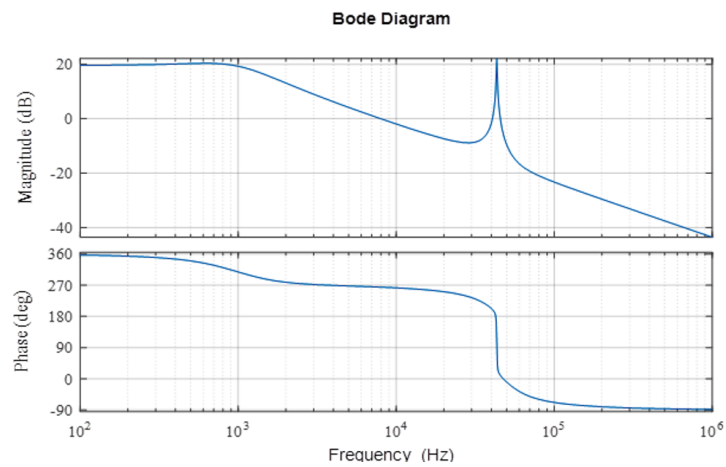FIGURE 15. Transient and steady state response of complex CBC.

FIGURE 16. Bode plot of control to output transfer function of complex CBC.

Duty ratio	Output voltage [V]	Load current [A]
0.3	2.47	0.3076
0.4	3.434	0.4266
0.5	5.44	0.6762
0.6	8.601	1.068
0.7	11.78	1.464

TABLE 4. Load current and output voltage for different duty rates.

4. RESULTS AND DISCUSSION

SSA and PWM switch modelling with EET technique for CBC (Section 2.2 and 2.3) are brainstormed, compared for different features and the results are summarized in Table 5. In SSA, a linearisation of all the components of the converter is performed, whereas in the PWM switch model method, only non-linear switching devices are linearised and linear components remain unchanged. In SSA technique, a set of differential equations are written which are further averaged with respect to the duty ratio function. The averaged equations are then linearised by using principle of perturbation, Laplace transform is applied to the linear state space model of CBC and the control to output transfer function is obtained. Unlike SSA technique, differential equations are not required in PWM switch modelling technique. Averaging and linearisation with the help of perturbation is accomplished using the PWM switch itself. Instead of Laplace transform, EET is applied to the linearised model of CBC to derive the control to output transfer function.

The SSA model of CBC is a systematic procedure involving mathematics without any circuit transformation. It involves complex mathematical transformations and a higher number of mathematical equations. In contrast, PWM switch modelling technique with EET consists of simple mathematical transformations. However, expertise is required for proper circuit transformations. Based on the parametric comparison (Table 5) of two analytical techniques, it is observed that SSA is better than the PWM with EET for a high-order circuit, due to systematic, straightforward procedural steps. PWM with EET for a high-order circuit requires a higher number of circuit transformations and a high expertise, which makes it time consuming and difficult.

Features	SSA technique	PWM switch modelling with EET
Analysis approach	Mathematical	Mainly circuit oriented
Structure of analysis	Systematic	Less systematic
Equivalent diagram	Not required	Required
Circuit transformation	Not required	Required
Number of mathematical transformations	More	Less
Number of mathematical equations	More	Less
Complexity of mathematical transformations	High	Low
Expertise required	Mathematical	Identification of PWM switch, changing the port sequences in case of indeterminacy and application of EET
Identification of PWM switch	Not required	Required
Extra Element Theorem	Not applicable	Applicable
Form of transfer function	Low entropy	Low entropy
The complexity of the modelling process	Low	High
Steady state analysis	Yes	Yes
Transient state analysis	Yes	Yes

TABLE 5. Results of comparative evaluation of the modelling techniques.

5. CONCLUSION

This paper presents a comparative study of two modelling techniques commonly used for modelling of DC-DC converters, which is first in its kind. The transfer functions of a complex CBC converter were developed using

state space averaging and PWM switch modelling with an extra element theorem and the simulation results were obtained. The state space modelling approach is purely mathematical and systematic. However, it involves complex mathematics for high-order circuits. The PWM switch modelling approach is mainly circuit oriented approach, which involves relatively simple mathematical transformations. However, circuit transformations become complex for a high-order circuit. A number of complex circuit transformations and identification of the PWM switch, changing the port sequences in the case of indeterminacy and application of EET make the PWM switch modelling approach a complex one as compared to the state space averaging approach.

REFERENCES

[1] S. H. Shete, P. M. Joshi. Analytical techniques for DC DC converters and 1Φ inverters: A comprehensive review. *Journal of The Institution of Engineers (India): Series B volume* **103**:1827–1844, 2022. https://doi.org/10.1007/s40031-022-00759-x.

[2] E. Vuthchhay, C. Bunlaksananusorn. Dynamic modeling of a zeta converter with state-space averaging technique. In *2008 5th International Conference on Electrical Engineering/Electronics, Computer, Telecommunications and Information Technology*, vol. 2, pp. 969–972. 2008. https://doi.org/10.1109/ECTICON.2008.4600593.

[3] S. Hegde, A. Izadian. A new SEPIC inverter: Small signal modeling. In *IECON 2013 – 39th Annual Conference of the IEEE Industrial Electronics Society*, pp. 240–245. 2013. https://doi.org/10.1109/IECON.2013.6699142.

[4] A. Davoudi, J. Jatskevich, T. De Rybel. Numerical state-space average-value modeling of PWM DC-DC converters operating in DCM and CCM. *IEEE Transactions on Power Electronics* **21**(4):1003–1012, 2006. https://doi.org/10.1109/TPEL.2006.876848.

[5] D. Czarkowski, M. K. Kazimierczuk. Energy-conservation approach to modeling PWM DC-DC converters. *IEEE Transactions on Aerospace and Electronic Systems* **29**(3):1059–1063, 1993. https://doi.org/10.1109/7.220955.

[6] M. Bartoli, A. Reatti, M. K. Kazimierczuk. Open loop small-signal control-to-output transfer function of PWM buck converter for CCM: modeling and measurements. In *Proceedings of 8th Mediterranean Electrotechnical Conference on Industrial Applications in Power Systems, Computer Science and Telecommunications (MELECON 96)*, vol. 3, pp. 1203–1206. 1996. https://doi.org/10.1109/MELCON.1996.551161.

[7] N. Kroutikova, C. A. Hernandez-Aramburo, T. C. Green. State-space model of grid-connected inverters under current control mode. *IET Electric Power Applications* **1**:329–338, 2007. https://doi.org/10.1049/iet-epa:20060276.

[8] H. Mashinchi Mahery, E. Babaei. Mathematical modeling of buck-boost dc-dc converter and investigation of converter elements on transient and steady state responses. *International Journal of Electrical Power & Energy Systems* **44**(1):949–963, 2013. https://doi.org/10.1016/j.ijepes.2012.08.035.

[9] S. Laali, H. M. Mahery. Buck DC-DC converter: Mathematical modeling and transient state analyzes. In *2012 3rd IEEE International Symposium on Power Electronics for Distributed Generation Systems (PEDG)*, pp. 661–667. 2012. https://doi.org/10.1109/PEDG.2012.6254073.

[10] M. Muntasir Nishat, M. A. Moin Oninda, F. Faisal, M. A. Hoque. Modeling, simulation and performance analysis of SEPIC converter using hysteresis current control and PI control method. In *2018 International Conference on Innovations in Science, Engineering and Technology (ICISET)*, pp. 7–12. 2018. https://doi.org/10.1109/ICISET.2018.8745619.

[11] V. Vorperian. Simplified analysis of PWM converters using model of PWM switch. Continuous conduction mode. *IEEE Transactions on Aerospace and Electronic Systems* **26**(3):490–496, 1990. https://doi.org/10.1109/7.106126.

[12] C. Basso. Switching-converter dynamic analysis with fast analytical techniques: Overview and applications. *IEEE Power Electronics Magazine* **4**(3):41–52, 2017. https://doi.org/10.1109/MPEL.2017.2718238.

[13] H. G. Tan Rodney, L. Y. H. Hoo. DC-DC converter modeling and simulation using state space approach. In *2015 IEEE Conference on Energy Conversion (CENCON)*, pp. 42–47. 2015. https://doi.org/10.1109/CENCON.2015.7409511.

[14] T. Polsky, Y. Horen, S. Bronshtein, D. Baimel. Transient and steady-state analysis of a SEPIC converter by an average state-space modelling. In *2018 IEEE 18th International Power Electronics and Motion Control Conference (PEMC)*, pp. 211–215. 2018. https://doi.org/10.1109/EPEPEMC.2018.8522000.

[15] B. P. Mokal, K. Vadirajacharya. Extensive modeling of DC-DC Cuk converter operating in continuous conduction mode. In *2017 International Conference on Circuit ,Power and Computing Technologies (ICCPCT)*, pp. 1–5. 2017. https://doi.org/10.1109/ICCPCT.2017.8074188.

[16] G. Kanimozhi, J. Meenakshi, V. T. Sreedevi. Small signal modeling of a DC-DC type double boost converter integrated with SEPIC converter using state space averaging approach. *Energy Procedia* **117**:835–846, 2017. https://doi.org/10.1016/j.egypro.2017.05.201.

[17] V. Eng, U. Pinsopon, C. Bunlaksananusorn. Modeling of a SEPIC converter operating in continuous conduction mode. In *2009 6th International Conference on Electrical Engineering/Electronics, Computer, Telecommunications and Information Technology*, pp. 136–139. 2009. https://doi.org/10.1109/ECTICON.2009.5136982.

[18] O. Kircioğlu, M. Ünlü, S. Çamur. Modeling and analysis of DC-DC SEPIC converter with coupled inductors. In *2016 International Symposium on Industrial Electronics (INDEL)*, pp. 1–5. 2016. `https://doi.org/10.1109/INDEL.2016.7797807`.

[19] N. Mohan, T. M. Undeland, W. P. Robbins. *Power Electronics – Converters, Applications and Design.* 3rd edition. John Wiley and Sons, 2013.

[20] C. Basso. *Linear Circuit Transfer Functions: An Introduction to Fast Analytical Techniques.* Wiley, Hoboken, NJ, 2016.

[21] V. Vorpérian. *Fast Analytical Techniques for Electrical and Electronic Circuits.* Cambridge University Press, Cambridge, U.K., 2002.

[22] S. K. Pidaparthy, B. Choi. Output impedance analysis of PWM DC-to-DC converters. In *2019 10th International Conference on Power Electronics and ECCE Asia (ICPE 2019 – ECCE Asia)*, pp. 849–855. 2019. `https://doi.org/10.23919/ICPE2019-ECCEAsia42246.2019.8796492`.

[23] B. Choi, D. Kim, D. Lee, et al. Analysis of input filter interactions in switching power converters. *IEEE Transactions on Power Electronics* **22**(2):452–460, 2007. `https://doi.org/10.1109/TPEL.2006.889925`.

[24] E. Can. PWM controlling of a new multi DC-DC converter circuit. *Technical Journal* **13**(2):116–122, 2019. `https://doi.org/10.31803/tg-20190427093441`.

[25] E. Can, H. H. Sayan. Different mathematical model for the chopper circuit. *Technical Journal* **10**(1-2):13–15, 2016. `https://hrcak.srce.hr/file/238913`.

[26] D. Maksimovic, S. Cuk. Switching converters with wide DC conversion range. *IEEE Transactions on Power Electronics* **6**(1):151–157, 1991. `https://doi.org/10.1109/63.65013`.

[27] M. M. Garg, Y. V. Hote, M. K. Pathak. Pi controller design of a dc-dc Zeta converter for specific phase margin and cross-over frequency. In *2015 10th Asian Control Conference (ASCC)*, pp. 1–6. 2015. `https://doi.org/10.1109/ASCC.2015.7244716`.